
Rethinking Assumptions in Deep Anomaly Detection

Lukas Ruff*

ML group
Technische Universität Berlin
10587 Berlin, Germany
lukas.ruff@tu-berlin.de

Robert A. Vandermeulen*

ML group
Technische Universität Berlin
10587 Berlin, Germany
vandermeulen@tu-berlin.de

Billy Joe Franks

Department of Computer Science
Technische Universität Kaiserslautern
67663 Kaiserslautern, Germany
b_franks12@cs.uni-kl.de

Klaus-Robert Müller

Google Research, Brain Team,
ML Group, TU Berlin,
MPII and Korea University
klaus-robert.mueller@tu-berlin.de

Marius Kloft

Department of Computer Science
Technische Universität Kaiserslautern
67663 Kaiserslautern, Germany
kloft@cs.uni-kl.de

Abstract

Though anomaly detection (AD) can be viewed as a classification problem (nominal vs. anomalous) it is usually treated in an unsupervised manner since one typically does not have access to, or it is infeasible to utilize, a dataset that sufficiently characterizes what it means to be “anomalous.” In this paper we present results demonstrating that this intuition surprisingly does not extend to deep AD on images. For a recent AD benchmark on ImageNet, classifiers trained to discern between normal samples and just a few (64) random natural images are able to outperform the current state of the art in deep AD. We find that this approach is also very effective at other common image AD benchmarks. Experimentally we discover that the multiscale structure of image data makes example anomalies exceptionally informative.

1 Introduction

Anomaly detection (AD) [22, 4, 27, 7, 52] is the task of determining if a sample is anomalous compared to a corpus of data. Recently there has been renewed interest in developing novel deep methods for AD [78, 17, 61, 58, 12, 56, 51, 47, 48, 73, 71]. Some of the best performing new AD methods for images were proposed in Golan and El-Yaniv [19] and Hendrycks et al. [26]. The aforementioned methods, like most previous works on AD, are performed in an *unsupervised* way: they only utilize an unlabeled corpus of mostly nominal data. While AD can be interpreted as a classification problem of “nominal vs. anomalous,” it is typically treated as an unsupervised problem due to the rather tricky issue of finding or constructing a dataset that somehow captures everything *different* from a nominal dataset.

One often has, in addition to a corpus of nominal data, access to some data which is known to be anomalous. There exist shallow [66, 70, 39, 21] and deep [36, 42, 25, 57] methods for incorporating

*equal contribution

anomalous data to augment unsupervised AD. This setting has been called “semi-supervised” AD [21, 57] or AD with “negative examples” [66]. In Hendrycks et al. [25] it was noted that, for an image AD problem, one has access to a virtually limitless amount of random natural images from the internet that are likely not nominal, and that such data should be utilized to improve unsupervised methods. They term the utilization of such data *outlier exposure* (OE). The state-of-the-art method presented in [26] utilizes tens of thousands of OE samples combined with a modified version of the method in [19] and is the best performing AD method to date on standard image AD benchmarks. For clarity, we here delineate the following three basic approaches to anomaly detection:

- **Unsupervised:** These are methods trained on a dataset of (mostly) nominal data. This is the classic and most common approach to AD.
- **Unsupervised OE:** These are adaptations of unsupervised methods to incorporate an auxiliary dataset that is not nominal. Elsewhere this is also called “semi-supervised” AD [21, 57] and AD with “negative examples” [66].
- **Supervised OE:** This is the approach of simply applying a standard classification method to discern between nominal data and an auxiliary dataset that is not nominal.

Using unsupervised OE rather than supervised OE to discern between the nominal data and known anomalies makes sense since the presented anomalies likely do not completely characterize “anomalousness.” This is illustrated in Figure 1 where we compare the decision regions of a supervised OE method vs. an unsupervised OE method. This intuition and the benefits of the unsupervised OE approach when incorporating known anomalies has also been observed in previous works [66, 39, 21, 57].

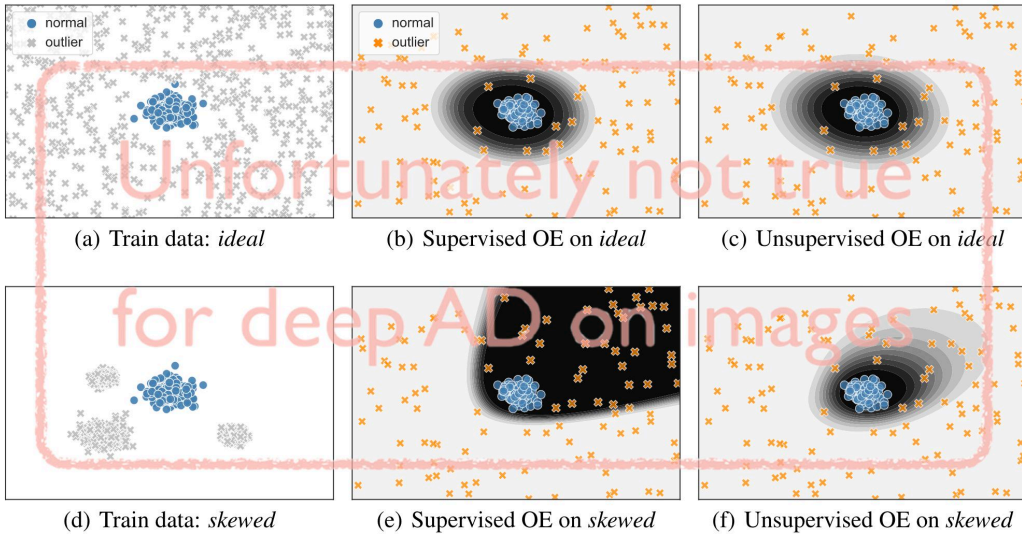


Figure 1: The decision boundaries of a supervised OE method (neural net with binary cross entropy) and an unsupervised OE method (neural net with loss introduced in Section 3) on two toy data settings: *ideal* ((a)–(c)) and *skewed* ((d)–(f)). The unsupervised OE method ((c) + (f)) learns compact decision regions following the so-called *concentration assumption* [62, 65] on the nominal class that is common in AD. Lacking this assumption, a supervised OE approach ((b) + (e)) learns decision regions that do not generalize well on this toy AD task. Our results suggest that this intuition does not hold for a deep approach to image AD, where supervised OE performs remarkably well.

In this paper we present experimental results that challenge the assumption that deep AD on images needs an unsupervised approach (with or without OE). We find that, using the same experimental OE setup as [26], a standard classifier is able to outperform all current state-of-the-art AD methods on the one vs. rest AD benchmarks on MNIST and CIFAR-10. The one vs. rest benchmark has been recommended as a general approach to experimentally validate AD methods [15]. This benchmark applied to the aforementioned datasets is used as a litmus test in virtually all deep AD papers published at top-tier venues; see for example [57, 26, 56, 19, 12, 2, 1, 49, 71, 5, 33]. Additionally we find that

remarkably few OE examples are necessary to characterize “anomalousness.” With 128 OE samples a classifier is competitive with state-of-the-art unsupervised methods on the CIFAR-10 one vs. rest benchmark. With only 64 OE samples a classifier outperforms all unsupervised methods, with or without OE, on a new one vs. rest ImageNet benchmark [26]. This test was recently proposed as a more challenging successor to the CIFAR-10 benchmark.

Our results seem to contradict the following pieces of common wisdom in deep learning and AD:

- Many (thousands) samples are needed for a deep method to understand a class of data [20].
- Anomalies are unconcentrated and thus inherently difficult to characterize with data [65, 8].

These points should imply that classification with few OE samples should be ineffective at deep AD. Instead, we find that relatively few random OE samples are necessary to yield state-of-the-art detection performance. In all of our experiments the nominal and OE data available during training are exactly those used in [26] and do not contain any representatives from the ground-truth anomaly classes. The OE data is not tailored to be representative of the anomalies used at test time.

We find that the key difference between classic AD and deep image AD is the presence of information at multiple spatial scales in images [46]. We hypothesize that each OE image contains multiple features at different scales which serve as examples of anomalousness. We present several experiments to support this claim. First the advantage of supervised OE over unsupervised OE is most evident on ImageNet, a high-resolution dataset able to encompass many spatial scales. This advantage declines for CIFAR-10, which has far less multiscale information, and is nonexistent for MNIST, which has essentially no multiscale information and unsupervised OE prevails. In further experiments we see that slightly blurring OE examples in our ImageNet experiments, thereby corrupting small scale features, causes a drastic reduction in performance. Once the OE samples are sufficiently blurred unsupervised OE becomes superior to supervised OE. Ultimately there appears to be two regimes for deep image AD: supervised OE, when the nominal class and OE examples contain sufficient multiscale information, and unsupervised OE, when this multiscale information is missing or there are exceptionally few OE samples. Finally, with a very large amount of OE examples where the benefit of OE becomes saturated, the approach matters little and both unsupervised OE and supervised OE meet the same performance asymptote.

2 Previous Work

While there exist many shallow methods for AD, it has been observed that these methods perform poorly for high-dimensional data [29, 37, 16, 17]. Deep approaches have been proposed to fill this gap. The most common approaches to deep AD employ autoencoders trained on nominal data, where samples not reconstructed well are deemed anomalous [24, 40, 59, 3, 64, 10, 55, 28]. Deep generative models have also been used to detect anomalies via a variety of methods [61, 12, 77], yet their effectiveness has been called into question [43].

A deep version of support vector data description (Deep SVDD) was proposed in Ruff et al. [56] where the authors replace the kernel feature map with a neural network which is learned during training. The network is trained to map nominal samples to a center \mathbf{c} . If $\phi(\cdot; \theta)$ is a neural network with parameters θ then the Deep SVDD objective is

$$\min_{\theta} \frac{1}{n} \sum_{i=1}^n \|\phi(\mathbf{x}_i; \theta) - \mathbf{c}\|^2. \quad (1)$$

Another recent avenue of research on deep AD uses self-supervision on images [18, 19, 72, 26]. In Golan and El-Yaniv [19] the authors use a composition of image transformations—including identity, rotations, flips, and translations—to create a self-supervised classification task. Every training sample is transformed using each of these transformations and a label is assigned to every transformed sample corresponding to the applied transformation. This creates a multi-class classification task for predicting image transformations. A network is then trained on this data to predict the applied transformation. For a test sample these transformations and network outputs are utilized to determine an anomaly score.

Complete code is made available under: <https://github.com/lukasruff/Classification-AD>

To our knowledge the best performing AD method on image data is the self-supervised approach from Hendrycks et al. [26] which extends Golan and El-Yaniv [19]’s method by using three classification heads to predict a combination of three types of transformations. They train their network on transformed nominal data as was done in Golan and El-Yaniv [19]. On a test sample the network’s certainty (how close to 1) on predicting correct transformations is used as an anomaly score, with certainty being a signifier that a sample is not anomalous. Essentially this assumes the network predictions to be less concentrated on the correct output for unfamiliar looking data. In that paper they validate their method on CIFAR-10 and ImageNet one vs. rest one-class learning benchmarks.

2.1 Auxiliary Data and the State of the Art for Deep AD on Images

Many deep learning methods have been proposed to incorporate the large amount of unorganized data that is now easily accessible on the web. A common way to use this data is via unsupervised learning. In the realm of NLP, word2vec [41] and more recent language models such as ELMo [50] or BERT [14] are now standard and responsible for significant improvements on various NLP tasks. For image tasks, using an auxiliary dataset for pretraining has been found to be effective [76]. Moreover many deep semi-supervised methods have been introduced to enhance classification performance via incorporating unlabeled data into training [35, 54, 44, 45].

The use of a large unstructured corpus of image data to improve deep AD was first proposed in Hendrycks et al. [25], where they call the general use of such data *outlier exposure* (OE). In Hendrycks et al. [26] the authors use OE to further improve existing self-supervised classification methods. They do this by training the aforementioned self-supervised methods to predict the uniform distribution for all transforms on OE samples, while leaving training on nominal samples unchanged. To our knowledge the AD method with OE presented in Hendrycks et al. [26] is the current state of the art on image data, beating previous unsupervised AD methods with or without OE.

2.2 Anomaly Detection as Binary Classification

Traditionally AD is understood as the problem of estimating the support (or level sets of the support) of the nominal data-generating distribution. This is also known as *density level set estimation* [53, 68]. The motivation for density level set estimation is the common assumption that nominal data is concentrated whereas anomalies are not concentrated [62]. Steinwart et al. [65] remark that the problem of density level set estimation can be interpreted as binary classification between the nominal and an anomalous distribution. Many of the classic AD methods (e.g., KDE or OC-SVM) implicitly assume the anomalies to follow a uniform, i.e. they make an uninformed prior assumption on the anomalous distribution [65]. These methods, as well as a binary classifier trained to discriminate between nominal samples and uniform noise, are asymptotically consistent density level set estimators [65, 69]. Obviously it is better to directly estimate the level set rather than introducing the auxiliary task of classifying against uniform noise. Such a classification approach is particularly ineffective and inefficient in high dimensions since it would require a massive amount of noise samples to properly fill the sample space. We find, however, that this intuition does not seem to extend to a deep approach to image anomaly detection when the anomalous examples are natural images.

3 Improving Deep Semi-Supervised Anomaly Detection

In Ruff et al. [57] the authors propose a method to extend Deep SVDD to incorporate known anomalies, which they call *Deep Semi-supervised Anomaly Detection* (Deep SAD). Deep SAD trains a network to concentrate nominal data near a predetermined center and maps anomalous samples away from that center. This is therefore an unsupervised OE approach to AD. Here we present a principled modification of Deep SAD based on cross-entropy classification that concentrates nominal samples. We call this method a *hypersphere classifier* (HSC). We found this modification to significantly improve upon the performance of Deep SAD and use it in our experiments as a representative of the unsupervised OE approach to AD.

Let $\mathcal{D} = \{(\mathbf{x}_1, y_1), (\mathbf{x}_2, y_2), \dots, (\mathbf{x}_n, y_n)\}$ be a dataset with $\mathbf{x}_i \in \mathbb{R}^d$ and $y \in \{0, 1\}$. Here $y = 1$ denotes a nominal data point and $y = 0$ denotes an anomaly. Let $\phi(\cdot; \theta) : \mathbb{R}^d \rightarrow \mathbb{R}^r$ be a neural network and $l : \mathbb{R}^r \rightarrow [0, 1]$ be a function which maps the output to a probabilistic score. Using

$\phi(\cdot; \theta)$ and $l(\cdot)$, the cross-entropy loss can be formulated as

$$-\frac{1}{n} \sum_{i=1}^n y_i \log l(\phi(\mathbf{x}_i; \theta)) + (1 - y_i) \log (1 - l(\phi(\mathbf{x}_i; \theta))). \quad (2)$$

For standard binary deep classifiers l is a linear layer followed by the sigmoid activation and the decision region for the mapped samples $\phi(\mathbf{x}_1; \theta), \dots, \phi(\mathbf{x}_n; \theta)$ is a half-space S . In this case the preimage of S , $\phi(\cdot; \theta)^{-1}(S)$, is not guaranteed to be compact. In order to enforce the preimage of our nominal decision region to be compact, thereby encouraging the mapped nominal data to be concentrated in a way similar to Deep SAD, we propose l to be a radial basis function. To construct a spherical decision boundary we let $l(\mathbf{z}) := \exp(-\|\mathbf{z}\|^2)$. In this case we have that (2) is equal to

$$\frac{1}{n} \sum_{i=1}^n y_i \|\phi(\mathbf{x}_i; \theta)\|^2 - (1 - y_i) \log \left(1 - \exp \left(-\|\phi(\mathbf{x}_i; \theta)\|^2 \right) \right). \quad (3)$$

If there are no anomalies, i.e. $y_i = 1$ for all i , then we have that (3) simplifies to $\frac{1}{n} \sum_{i=1}^n \|\phi(\mathbf{x}_i; \theta)\|^2$. Thus, for $c = 0$ we recover the Deep SVDD loss (1) as a special case. Similar to Deep SVDD and Deep SAD, we define our anomaly score as $s(\mathbf{x}) := \|\phi(\mathbf{x}; \theta)\|^2$.

Motivated by robust statistics [23, 30] we also considered replacing l with other radial functions where the squared-norm is replaced with a robust alternative. We found that using a pseudo-Huber loss [9] $l(\mathbf{z}) = \exp(-h(\mathbf{z}))$ that interpolates between squared and absolute value penalization yields the best results: $h(\mathbf{z}) = \sqrt{\|\mathbf{z}\|^2 + 1} - 1$. We include a sensitivity analysis comparing various choices of norms for the hypersphere classifier in Appendix B.

4 Experiments

One vs. Rest Benchmark We consider the one vs. rest evaluation setting, which is a ubiquitous benchmark in deep AD literature [57, 26, 56, 19, 12, 2, 1, 49, 71, 5, 33]. The one vs. rest evaluation constructs AD settings from classification datasets (e.g., MNIST) by considering the “one” class (e.g., digit 0) as being nominal and the “rest” classes (e.g., digits 1–9) as being anomalous at test time. In each experiment, we train a model using only the training set of the nominal class as well as random samples from an OE set (e.g., EMNIST-Letters) which is disjoint from the ground-truth anomaly classes of the benchmark. We use the same OE auxiliary datasets as suggested in previous literature [25, 26]. We then evaluate performance using the common Area Under the ROC curve (AUC) on the one vs. rest test sets. This is repeated for each class and for multiple random seeds.

Datasets

MNIST: The ten MNIST classes are used as our one vs. rest classes. For OE we use the EMNIST-Letters dataset [11] which shares no common classes with MNIST.

CIFAR-10: The ten CIFAR-10 classes are used as our one vs. rest classes. For OE we use 80 Million Tiny Images (80MTI) [67] with CIFAR-10 and CIFAR-100 images removed. This is in accordance with the experimental setup used in Hendrycks et al. [26]. In one of our ablation experiments we alternatively consider using CIFAR-100 as the OE dataset.

ImageNet: We use thirty classes from the ImageNet-1K [13] dataset as the one vs. rest classes. These are the same classes as were used in Hendrycks et al. [26]. For OE we use the ImageNet-22K dataset with the ImageNet-1K classes removed. This again follows [26].

Methods We present results from all recent deep AD methods that achieve state-of-the-art performance on the one vs. rest benchmarks.

Unsupervised: We use Deep SVDD* [56], Geo* [19], Geo+* [26], as well as IT* [28] as shorthands for the state-of-the-art unsupervised methods. We also report the results of a shallow SVDD* [66, 63] baseline.

Unsupervised OE: We implement the Hypersphere Classifier (HSC) from Section 3 and Deep SAD [57] as unsupervised OE methods. We also report the results from the state-of-the-art unsupervised OE Geo+* variant [26].

Supervised OE: We consider a standard binary cross-entropy classifier which we refer to as BCE. Moreover we implement the Focal loss classifier [38], a BCE variant which specifically addresses class imbalance and was also presented in Hendrycks et al. [26]. We refer to the results from our implementation as Focal and the results from [26] as Focal*. We set $\gamma = 2$ as recommended in the original work [38].

Network Architectures and Optimization We always use the same underlying network $\phi(\cdot; \theta)$ in each experimental setting for our HSC, Deep SAD, Focal, and BCE implementations to control architectural effects. For Focal and BCE, the output of the network $\phi(\cdot; \theta)$ is followed by a linear layer with sigmoid activation. For the experiments on MNIST and CIFAR-10 we use standard LeNet-style networks having three convolutional layers followed by two fully connected layers. We use batch normalization [31] and (leaky) ReLU activations in these networks. For our experiments on ImageNet we use the same WideResNet [75] as [26], which has ResNet-18 as its architectural backbone. We use Adam [34] for optimization and balance every batch to contain 128 nominal and 128 OE samples during training. For data augmentation, we use standard color jitter, random cropping, horizontal flipping, and Gaussian pixel noise. We report full details in Appendix D.

Varying the OE Size For HSC and BCE we also present extensive experiments showing the performance as the OE training set size is varied on a log scale from $2^0 = 1$ sample to using the maximal amount of OE data such that OE samples are never seen twice during training. If the amount of OE data in a subset is less than the OE batch size of 128, we sample with replacement from the subset. Note that applying data augmentation introduces some variety to the OE set, even in the extreme case of having only $2^0 = 1$ sample.

4.1 Results on the CIFAR-10 Anomaly Detection Benchmark

The results on the CIFAR-10 one vs. rest benchmark for all classes are shown in Table 1. We observe a comparable state-of-the-art detection performance for the unsupervised OE methods Geo+* and HSC. Interestingly, the supervised Focal and BCE methods also have competitive detection performance, with BCE attaining the best mean AUC overall. To better understand the informativeness of OE for unsupervised and supervised approaches, we compare the performance of HSC and BCE while varying the OE set size. The results in Figure 2 demonstrate that surprisingly few OE samples already yield very competitive detection performance.

Table 1: Detection performance in mean AUC in % (over 10 seeds) on the CIFAR-10 one vs. rest benchmark using 80MTI as OE. (* are results from the literature)

Class	Unsupervised					Unsupervised OE			Supervised OE		
	SVDD*	Deep SVDD*	Geo*	IT*	Geo+*	Geo+*	Deep SAD	HSC	Focal*	Focal	BCE
Airplane	65.6	61.7	74.7	78.5	77.5	90.4	94.2	96.3	87.6	95.9	96.4
Automobile	40.9	65.9	95.7	89.8	96.9	99.3	98.1	98.7	93.9	98.7	98.8
Bird	65.3	50.8	78.1	86.1	87.3	93.7	89.8	92.7	78.6	92.3	93.0
Cat	50.1	59.1	72.4	77.4	80.9	88.1	87.4	89.8	79.9	88.8	90.0
Deer	75.2	60.9	87.8	90.5	92.7	97.4	95.0	96.6	81.7	96.6	97.1
Dog	51.2	65.7	87.8	84.5	90.2	94.3	93.0	94.2	85.6	94.1	94.2
Frog	71.8	67.7	83.4	89.2	90.9	97.1	96.9	97.9	93.3	97.8	98.0
Horse	51.2	67.3	95.5	92.9	96.5	98.8	96.8	97.6	87.9	97.6	97.6
Ship	67.9	75.9	93.3	92.0	95.2	98.7	97.1	98.2	92.6	98.0	98.1
Truck	48.5	73.1	91.3	85.5	93.3	98.5	96.2	97.4	92.1	97.5	97.7
Mean AUC	58.8	64.8	86.0	86.6	90.1	95.6	94.5	95.9	87.3	95.8	96.1

4.2 Results on the ImageNet Anomaly Detection Benchmark

The results for the ImageNet one vs. rest benchmark are shown in Table 2. Due to space constraints, we only report the mean AUC over all thirty classes here and refer to Appendix E for the individual class results. We report Geo+* and Focal* from [26], where this benchmark was recently introduced. Deep SAD, HSC, Focal, and BCE all outperform the current state of the art, Geo+* [26], by a surprisingly wide margin. We are unsure as to why the Focal* results from [26] are so poor since their experimental code is not public. We found performance to be insensitive to the choice of γ in the Focal loss (see Appendix C). Not balancing the number of nominal and OE samples in each batch might also cause this gap. It may also be possible that the Focal loss experiment in [26] is erroneous.

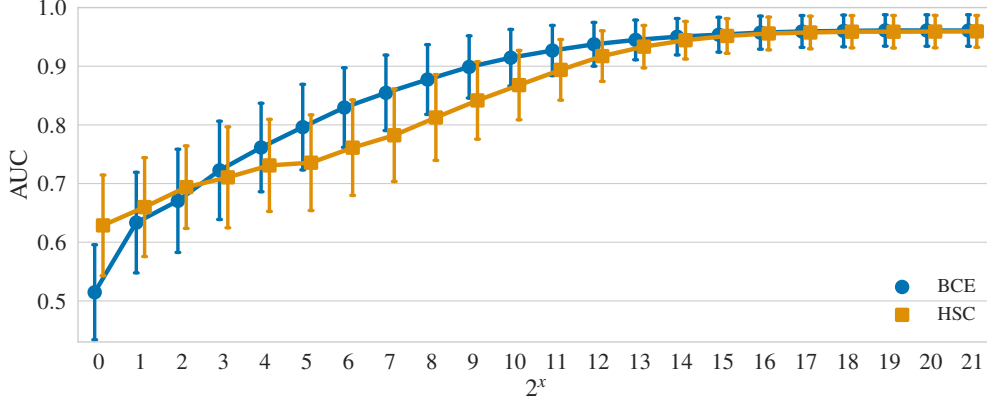


Figure 2: Detection performance in mean AUC in % (over 10 classes with 10 seeds per class) on the CIFAR-10 one vs. rest benchmark when varying the number of 80MTI OE samples.

We again compare the performance of HSC and BCE while varying the OE set size. The results are in Figure 3. As before we see that there is a transition from HSC to BCE performing best, which can be understood as a transition from unsupervised OE to supervised OE. Remarkably, classification beats previous methods with only 64 OE samples.

Table 2: Detection performance in mean AUC in % (over 30 classes and 10 seeds) on the ImageNet-1K one vs. rest benchmark using ImageNet-22K (with the 1K classes removed) as OE. (* are results from the literature)

	Unsupervised OE			Supervised OE		
	Geo+*	Deep SAD	HSC	Focal*	Focal	BCE
Mean AUC	85.7	96.7	97.3	56.1	97.5	97.7

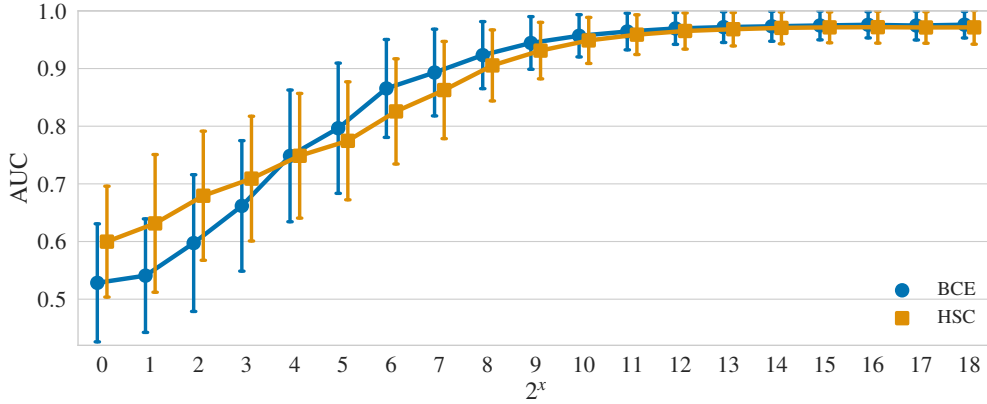


Figure 3: Detection performance in mean AUC in % (over 30 classes with 5 seeds per class) on the ImageNet-1K one vs. rest benchmark when varying the number of ImageNet-22K OE samples.

4.3 Diversity of the Outlier Exposure Data

Here we evaluate how data diversity influences detection performance for unsupervised and supervised OE, again comparing HSC to BCE. For this purpose, instead of 80MTI, we now use CIFAR-100 as OE varying the number of anomaly classes available for the CIFAR-10 benchmark. We further evaluate the methods on the MNIST one vs. rest benchmark where EMNIST-Letters is used as the OE dataset. For both experiments the OE data is varied by choosing k classes at random for each random seed and using the union of these classes as the OE dataset.

The results are presented in Figure 4. As expected, the performance increases with the diversity of the OE dataset. Interestingly, drawing OE samples from just $k = 1$ class, i.e. binary classification between the nominal class and a single OE class (which is not present as an anomaly class at test time!) already yields good detection performance on the CIFAR-10 benchmark. For example training a standard classification network to discern between automobiles and beavers performs competitively as an automobile anomaly detector, even when no beavers are present as anomalies during test time.

For the MNIST experiment we see that HSC outperforms BCE for any number of classes. We hypothesize that this is due to the lack of multiscale spatial structure in the MNIST and EMNIST datasets. This intuition is consistent with the classic understanding of AD mentioned in the introduction.

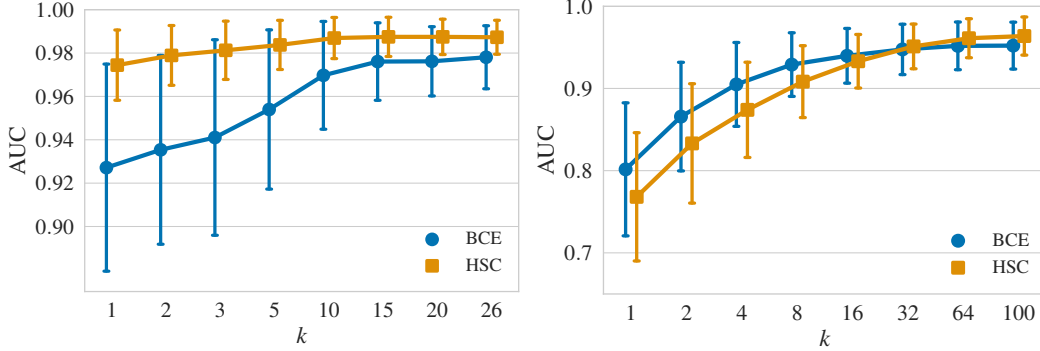


Figure 4: Detection performance in mean AUC in % (over 10 classes with 10 seeds per class) on the MNIST with EMNIST-Letters OE (left) and CIFAR-10 with CIFAR-100 OE (right) one vs. rest benchmarks when varying the number of k classes that comprise the OE dataset.

4.4 Removing Multiscale Information

To investigate the hypothesis that the exceptional informativeness of OE samples is due to the multiscale structure of natural images, we perform an experiment which removes small scale features from the OE dataset. To do this we compare the detection performance of HSC and BCE on the ImageNet one vs. rest task while increasingly blurring the OE samples with a Gaussian filter. The blurring gradually removes the small scale (high frequency) features from the OE data.

We see in Figure 5 that performance drops quickly with even a small amount of blurring. With sufficient blurring the unsupervised OE method (HSC) performs best. We provide the results for MNIST and CIFAR-10 in Appendix A, where we observe a similar decrease in performance for CIFAR-10. For MNIST however, HSC outperforms BCE at any degree of blurring and retains a good performance. This again supports our hypothesis of two regimes in deep image AD.

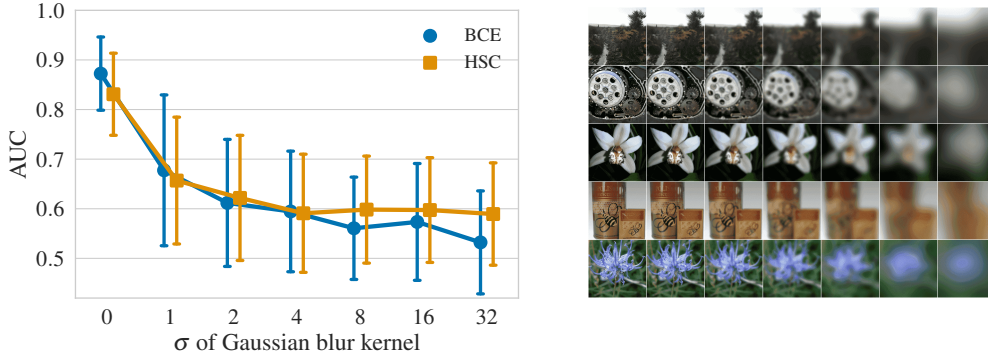


Figure 5: Detection performance in mean AUC on ImageNet when the OE data samples become increasingly blurred with a Gaussian kernel for having $2^6 = 64$ OE samples (left). An example of the various degrees of blurring is shown on the right. The abrupt decrease in AUC suggests the exceptional informativeness of OE on images is due to the multiscale structure of images.

5 Discussion and Conclusion

We have demonstrated that deep AD on images displays a phenomenon which is quite different from what is expected in classic AD. Compared to classic AD, a few example outliers are exceptionally informative on common image AD benchmarks. Furthermore, we have shown that this phenomenon is tied to the multiscale nature of natural images.

We do not claim that a supervised OE approach is *the* solution to AD in general, or that there is no utility for the unsupervised OE approach. However, it does appear that it may be time for the community to move to different or more challenging tasks to gauge the significance of deep AD works. One could concoct a more difficult variant of the one vs. rest benchmark: for example reporting the AUC of the nominal class vs. the worst anomalous class (one vs. worst). Alternatively there exist real world AD datasets where the nominal samples are less diverse and the anomalies more subtle. This setting is found in industrial quality control [6] and medical diagnosis [74], for example. In these settings, annotating the anomalous locations in an image is often desirable. This yields a markedly different problem than simply detecting anomalies and connects deep AD to explainable and interpretable deep learning [60, 32].

Acknowledgments and Disclosure of Funding

LR acknowledges support by the German Federal Ministry of Education and Research (BMBF) in the project ALICE III (01IS18049B). RV acknowledges support by the Berlin Institute for the Foundations of Learning and Data (BIFOLD) sponsored by the German Federal Ministry of Education and Research (BMBF). KRM was supported in part by the Institute for Information & Communications Technology Promotion and funded by the Korea government (MSIT) (No. 2017-0-01779), and was partly supported by the German Federal Ministry of Education and Research (BMBF) under Grants 01IS14013A-E, 01GQ1115, 01GQ0850, 01IS18025A and 01IS18037A; the German Research Foundation (DFG) under Grant Math+, EXC 2046/1, Project ID 390685689. MK and BJF acknowledge support by the German Research Foundation (DFG) award KL 2698/2-1 and by the German Federal Ministry of Science and Education (BMBF) awards 031L0023A, 01IS18051A, and 031B0770E. Part of the work was done while MK was a sabbatical visitor of the DASH Center at the University of Southern California.

References

- [1] D. Abati, A. Porrello, S. Calderara, and R. Cucchiara. Latent space autoregression for novelty detection. In *2019 IEEE/CVF Conference on Computer Vision and Pattern Recognition (CVPR)*, pages 481–490, 2019.
- [2] S. Akcay, A. Atapour-Abarghouei, and T. P. Breckon. Ganomaly: Semi-supervised anomaly detection via adversarial training. In C. V. Jawahar, H. Li, G. Mori, and K. Schindler, editors, *Computer Vision – ACCV 2018*, pages 622–637, Cham, 2019. Springer International Publishing. ISBN 978-3-030-20893-6.
- [3] J. An and S. Cho. Variational autoencoder based anomaly detection using reconstruction probability. *Special Lecture on IE*, 2(1), 2015.
- [4] V. Barnett and T. Lewis. *Outliers in Statistical Data*. Wiley, 3rd edition, 1994.
- [5] L. Bergman and Y. Hoshen. Classification-based anomaly detection for general data. In *International Conference on Learning Representations*, 2020.
- [6] P. Bergmann, M. Fauser, D. Sattlegger, and C. Steger. Mvtec ad – a comprehensive real-world dataset for unsupervised anomaly detection. In *The IEEE Conference on Computer Vision and Pattern Recognition (CVPR)*, June 2019.
- [7] V. Chandola, A. Banerjee, and V. Kumar. Anomaly detection: A survey. *ACM computing surveys (CSUR)*, 41(3):15, 2009.
- [8] O. Chapelle, B. Schölkopf, and A. Zien. Semi-supervised learning. *IEEE Transactions on Neural Networks*, 20(3):542–542, 2009.
- [9] P. Charbonnier, L. Blanc-Féraud, G. Aubert, and M. Barlaud. Deterministic edge-preserving regularization in computed imaging. *IEEE Transactions on image processing*, 6(2):298–311, 1997.

- [10] J. Chen, S. Sathe, C. C. Aggarwal, and D. S. Turaga. Outlier Detection with Autoencoder Ensembles. In *SDM*, pages 90–98, 2017.
- [11] G. Cohen, S. Afshar, J. Tapson, and A. van Schaik. EMNIST: an extension of MNIST to handwritten letters. *CoRR*, abs/1702.05373, 2017.
- [12] L. Deecke, R. Vandermeulen, L. Ruff, S. Mandt, and M. Kloft. Image anomaly detection with generative adversarial networks. In *Joint European Conference on Machine Learning and Knowledge Discovery in Databases*, pages 3–17. Springer, 2018.
- [13] J. Deng, W. Dong, R. Socher, L.-J. Li, K. Li, and L. Fei-Fei. ImageNet: A Large-Scale Hierarchical Image Database. In *CVPR09*, 2009.
- [14] J. Devlin, M.-W. Chang, K. Lee, and K. Toutanova. BERT: Pre-training of deep bidirectional transformers for language understanding. *arXiv:1810.04805*, 2018.
- [15] A. F. Emmott, S. Das, T. Dietterich, A. Fern, and W.-K. Wong. Systematic construction of anomaly detection benchmarks from real data. In *Proceedings of the ACM SIGKDD Workshop on Outlier Detection and Description*, page 16–21, 2013.
- [16] S. Erfani, M. Baktashmotlagh, S. Rajasegarar, S. Karunasekera, and C. Leckie. R1SVM: a randomised nonlinear approach to large-scale anomaly detection. In *Twenty-Ninth AAAI Conference on Artificial Intelligence*, pages 432–438, 2015.
- [17] S. M. Erfani, S. Rajasegarar, S. Karunasekera, and C. Leckie. High-dimensional and large-scale anomaly detection using a linear one-class SVM with deep learning. *Pattern Recognition*, 58:121–134, 2016.
- [18] S. Gidaris, P. Singh, and N. Komodakis. Unsupervised representation learning by predicting image rotations. *arXiv preprint arXiv:1803.07728*, 2018.
- [19] I. Golan and R. El-Yaniv. Deep anomaly detection using geometric transformations. In *Advances in Neural Information Processing Systems*, pages 9758–9769, 2018.
- [20] I. Goodfellow, Y. Bengio, and A. Courville. *Deep Learning*. MIT Press, 2016. <http://www.deeplearningbook.org>.
- [21] N. Görnitz, M. Kloft, K. Rieck, and U. Brefeld. Toward supervised anomaly detection. *Journal of Artificial Intelligence Research*, 46:235–262, 2013.
- [22] F. E. Grubbs. Procedures for detecting outlying observations in samples. *Technometrics*, 11(1):1–21, 1969.
- [23] F. R. Hampel, E. M. Ronchetti, P. J. Rousseeuw, and W. A. Stahel. *Robust Statistics: The Approach Based on Influence Functions*. John Wiley & Sons, 2005.
- [24] S. Hawkins, H. He, G. Williams, and R. Baxter. Outlier detection using replicator neural networks. In *International Conference on Data Warehousing and Knowledge Discovery*, pages 170–180. Springer, 2002.
- [25] D. Hendrycks, M. Mazeika, and T. G. Dietterich. Deep anomaly detection with outlier exposure. In *ICLR*, 2019.
- [26] D. Hendrycks, M. Mazeika, S. Kadavath, and D. Song. Using self-supervised learning can improve model robustness and uncertainty. In *Advances in Neural Information Processing Systems*, pages 15637–15648, 2019.
- [27] V. Hodge and J. Austin. A survey of outlier detection methodologies. *Artificial Intelligence Review*, 22(2): 85–126, 2004.
- [28] C. Huang, J. Cao, F. Ye, M. Li, Y. Zhang, and C. Lu. Inverse-transform autoencoder for anomaly detection. *arXiv preprint arXiv:1911.10676*, 2019.
- [29] F. J. Huang and Y. LeCun. Large-scale learning with svm and convolutional for generic object categorization. In *2006 IEEE Computer Society Conference on Computer Vision and Pattern Recognition (CVPR’06)*, volume 1, pages 284–291. IEEE, 2006.
- [30] P. J. Huber and E. M. Ronchetti. *Robust Statistics*. John Wiley & Sons, 2nd edition, 2009.
- [31] S. Ioffe and C. Szegedy. Batch Normalization: Accelerating Deep Network Training by Reducing Internal Covariate Shift. In *ICML*, pages 448–456, 2015.

- [32] J. Kauffmann, K.-R. Müller, and G. Montavon. Towards explaining anomalies: a deep taylor decomposition of one-class models. *Pattern Recognition*, 101:107198, 2020.
- [33] K. H. Kim, S. Shim, Y. Lim, J. Jeon, J. Choi, B. Kim, and A. S. Yoon. Rapp: Novelty detection with reconstruction along projection pathway. In *International Conference on Learning Representations*, 2020.
- [34] D. P. Kingma and J. Ba. Adam: A Method for Stochastic Optimization. *arXiv:1412.6980*, 2014.
- [35] D. P. Kingma, S. Mohamed, D. J. Rezende, and M. Welling. Semi-supervised learning with deep generative models. In *NIPS*, pages 3581–3589, 2014.
- [36] B. Kiran, D. Thomas, and R. Parakkal. An overview of deep learning based methods for unsupervised and semi-supervised anomaly detection in videos. *Journal of Imaging*, 4(2):36, 2018.
- [37] H.-P. Kriegel, M. Schubert, and A. Zimek. Angle-based outlier detection in high-dimensional data. In *Proceedings of the 14th ACM SIGKDD international conference on Knowledge discovery and data mining*, pages 444–452, 2008.
- [38] T.-Y. Lin, P. Goyal, R. Girshick, K. He, and P. Dollar. Focal loss for dense object detection. In *The IEEE International Conference on Computer Vision (ICCV)*, Oct 2017.
- [39] Y. Liu and Y. F. Zheng. Minimum enclosing and maximum excluding machine for pattern description and discrimination. In *ICPR*, pages 129–132, 2006.
- [40] J. Masci, U. Meier, D. Cireşan, and J. Schmidhuber. Stacked convolutional auto-encoders for hierarchical feature extraction. In *International conference on artificial neural networks*, pages 52–59. Springer, 2011.
- [41] T. Mikolov, I. Sutskever, K. Chen, G. S. Corrado, and J. Dean. Distributed representations of words and phrases and their compositionality. In *NIPS*, pages 3111–3119, 2013.
- [42] E. Min, J. Long, Q. Liu, J. Cui, Z. Cai, and J. Ma. SU-IDS: A semi-supervised and unsupervised framework for network intrusion detection. In *International Conference on Cloud Computing and Security*, pages 322–334, 2018.
- [43] E. Nalisnick, A. Matsukawa, Y. W. Teh, D. Gorur, and B. Lakshminarayanan. Do deep generative models know what they don’t know? In *ICLR*, 2019.
- [44] A. Odena. Semi-supervised learning with generative adversarial networks. *arXiv:1606.01583*, 2016.
- [45] A. Oliver, A. Odena, C. Raffel, E. D. Cubuk, and I. J. Goodfellow. Realistic evaluation of deep semi-supervised learning algorithms. *arXiv:1804.09170*, 2018.
- [46] B. A. Olshausen and D. J. Field. Emergence of simple-cell receptive field properties by learning a sparse code for natural images. *Nature*, 381(6583):607–609, Jun 1996.
- [47] G. Pang, C. Shen, and A. van den Hengel. Deep anomaly detection with deviation networks. In *KDD*, pages 353–362, 2019.
- [48] P. Perera and V. M. Patel. Learning deep features for one-class classification. *IEEE Transactions on Image Processing*, 28(11):5450–5463, 2019.
- [49] P. Perera, R. Nallapati, and B. Xiang. Ocgan: One-class novelty detection using gans with constrained latent representations. In *2019 IEEE/CVF Conference on Computer Vision and Pattern Recognition (CVPR)*, pages 2893–2901, 2019.
- [50] M. Peters, M. Neumann, M. Iyyer, M. Gardner, C. Clark, K. Lee, and L. Zettlemoyer. Deep contextualized word representations. In *Proceedings of the 2018 Conference of the North American Chapter of the Association for Computational Linguistics: Human Language Technologies, Volume 1 (Long Papers)*, pages 2227–2237, New Orleans, Louisiana, June 2018. Association for Computational Linguistics.
- [51] S. Pidhorskyi, R. Almohsen, and G. Doretto. Generative probabilistic novelty detection with adversarial autoencoders. In *NeurIPS*, pages 6822–6833, 2018.
- [52] M. A. Pimentel, D. A. Clifton, L. Clifton, and L. Tarassenko. A review of novelty detection. *Signal Processing*, 99:215–249, 2014.
- [53] W. Polonik. Measuring mass concentrations and estimating density contour clusters-an excess mass approach. *The Annals of Statistics*, 23(3):855–881, 1995.

- [54] A. Rasmus, M. Berglund, M. Honkala, H. Valpola, and T. Raiko. Semi-supervised learning with ladder networks. In *NIPS*, pages 3546–3554, 2015.
- [55] C. Richter and N. Roy. Safe visual navigation via deep learning and novelty detection. In *Robotics: Science and Systems Foundation XIII*, 2017.
- [56] L. Ruff, R. Vandermeulen, N. Goernitz, L. Deecke, S. A. Siddiqui, A. Binder, E. Müller, and M. Kloft. Deep one-class classification. In *International Conference on Machine Learning*, pages 4393–4402, 2018.
- [57] L. Ruff, R. A. Vandermeulen, N. Görnitz, A. Binder, E. Müller, K.-R. Müller, and M. Kloft. Deep semi-supervised anomaly detection. In *International Conference on Learning Representations*, 2020.
- [58] M. Sabokrou, M. Khalooei, M. Fathy, and E. Adeli. Adversarially learned one-class classifier for novelty detection. In *CVPR*, pages 3379–3388, 2018.
- [59] M. Sakurada and T. Yairi. Anomaly detection using autoencoders with nonlinear dimensionality reduction. In *Proceedings of the MLSDA 2014 2nd Workshop on Machine Learning for Sensory Data Analysis*, pages 4–11, 2014.
- [60] W. Samek, G. Montavon, S. Lapuschkin, C. J. Anders, and K.-R. Müller. Toward interpretable machine learning: Transparent deep neural networks and beyond. *arXiv preprint arXiv:2003.07631*, 2020.
- [61] T. Schlegl, P. Seeböck, S. M. Waldstein, U. Schmidt-Erfurth, and G. Langs. Unsupervised anomaly detection with generative adversarial networks to guide marker discovery. In *International conference on information processing in medical imaging*, pages 146–157. Springer, 2017.
- [62] B. Schölkopf and A. J. Smola. *Learning with Kernels*. MIT press, 2002.
- [63] B. Schölkopf, J. C. Platt, J. Shawe-Taylor, A. J. Smola, and R. C. Williamson. Estimating the Support of a High-Dimensional Distribution. *Neural computation*, 13(7):1443–1471, 2001.
- [64] P. Seeböck, S. Waldstein, S. Klimesch, B. S. Gerendas, R. Donner, T. Schlegl, U. Schmidt-Erfurth, and G. Langs. Identifying and categorizing anomalies in retinal imaging data. *arXiv preprint arXiv:1612.00686*, 2016.
- [65] I. Steinwart, D. Hush, and C. Scovel. A classification framework for anomaly detection. *Journal of Machine Learning Research*, 6(Feb):211–232, 2005.
- [66] D. M. J. Tax. *One-class classification*. PhD thesis, Delft University of Technology, 2001.
- [67] A. Torralba, R. Fergus, and W. T. Freeman. 80 million tiny images: A large data set for nonparametric object and scene recognition. *IEEE transactions on pattern analysis and machine intelligence*, 30(11):1958–1970, 2008.
- [68] A. B. Tsybakov. On nonparametric estimation of density level sets. *The Annals of Statistics*, 25(3):948–969, 1997.
- [69] R. Vert and J.-P. Vert. Consistency and convergence rates of one-class svms and related algorithms. *Journal of Machine Learning Research*, 7(May):817–854, 2006.
- [70] J. Wang, P. Neskovic, and L. N. Cooper. Pattern classification via single spheres. In *International Conference on Discovery Science*, pages 241–252. Springer, 2005.
- [71] J. Wang, S. Sun, and Y. Yu. Multivariate triangular quantile maps for novelty detection. In *Advances in Neural Information Processing Systems 32*, pages 5060–5071, 2019.
- [72] S. Wang, Y. Zeng, X. Liu, E. Zhu, J. Yin, C. Xu, and M. Kloft. Effective end-to-end unsupervised outlier detection via inlier priority of discriminative network. In H. M. Wallach, H. Larochelle, A. Beygelzimer, F. d’Alché-Buc, E. B. Fox, and R. Garnett, editors, *Advances in Neural Information Processing Systems 32: Annual Conference on Neural Information Processing Systems 2019, NeurIPS 2019, 8-14 December 2019, Vancouver, BC, Canada*, pages 5960–5973, 2019.
- [73] S. Wang, Y. Zeng, X. Liu, E. Zhu, J. Yin, C. Xu, and M. Kloft. Effective end-to-end unsupervised outlier detection via inlier priority of discriminative network. In *NeurIPS*, pages 5960–5973, 2019.
- [74] S. Yoo, I. Gujrathi, M. A. Haider, and F. Khalvati. Prostate cancer detection using deep convolutional neural networks. *Scientific Reports*, 9(1):19518, Dec 2019.
- [75] S. Zagoruyko and N. Komodakis. Wide residual networks. In *BMVC*, 2016.

- [76] M. D. Zeiler and R. Fergus. Visualizing and understanding convolutional networks. In *European conference on computer vision*, pages 818–833. Springer, 2014.
- [77] H. Zenati, C. S. Foo, B. Lecouat, G. Manek, and V. R. Chandrasekhar. Efficient gan-based anomaly detection. *arXiv preprint arXiv:1802.06222*, 2018.
- [78] S. Zhai, Y. Cheng, W. Lu, and Z. Zhang. Deep structured energy based models for anomaly detection. In *ICML*, volume 48, pages 1100–1109, 2016.

A Removing Multiscale Information on MNIST and CIFAR-10

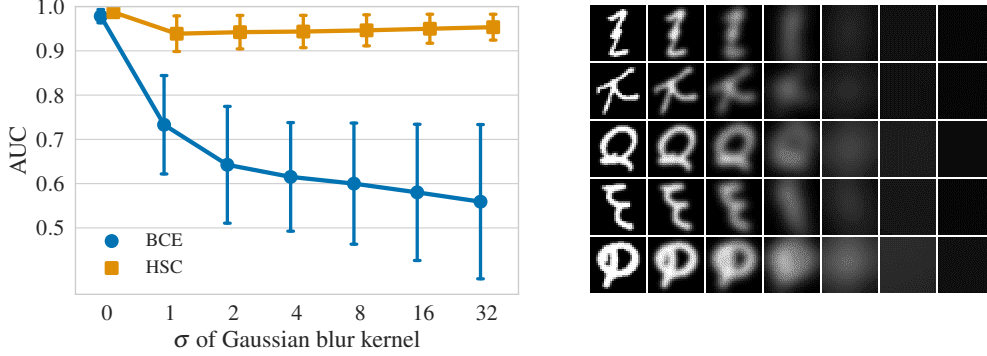


Figure 6: Detection performance in mean AUC on the MNIST one vs. rest benchmark when the EMNIST OE data samples become increasingly blurred with a Gaussian kernel (left). An example of blurring some EMNIST OE samples is shown to the right. We see that HSC clearly outperforms BCE on MNIST, a dataset which has essentially no multiscale information.

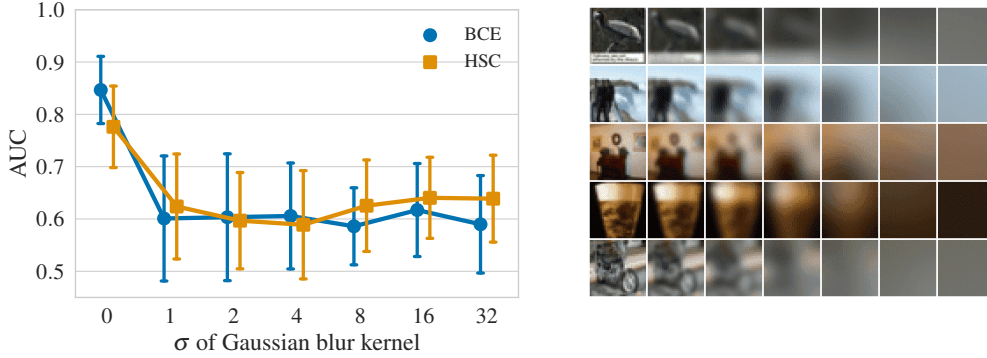


Figure 7: Detection performance in mean AUC on the CIFAR-10 one vs. rest benchmark when the 80MTI OE data samples become increasingly blurred with a Gaussian kernel for having $2^7 = 128$ OE samples (left). An example of blurring some 80MTI OE samples is shown to the right. The rapid decrease in AUC on CIFAR-10 again suggests that the informativeness of OE on images is due to the multiscale structure of images.

B Sensitivity Analysis for the Hypersphere Classifier

Here we show results for the Hypersphere Classifier (HSC) we introduced in Section 3 when varying the radial function $l(z) = \exp(-h(z))$. For this we run the CIFAR-10 one vs. rest benchmark with 80MTI OE experiment as presented in Table 1 in the main paper for different functions $h : \mathbb{R}^r \rightarrow [0, \infty), z \mapsto h(z)$. We also alter training to be with or without data augmentation in these experiments. The results are presented in Table 3. We see that data augmentation leads to an improvement in performance even in this case where we have the full 80MTI dataset as OE. HSC shows the overall best performance with data augmentation and using the robust Pseudo-Huber loss $h(z) = \sqrt{\|z\|^2 + 1} - 1$.

C Focal Loss With Varying γ

Here we include results showing how mean AUC detection performance changes with γ on the Focal loss. Since we balance every batch to contain 128 nominal and 128 OE samples during training, we

Table 3: Detection performance in mean AUC in % (over 10 seeds) on the CIFAR-10 one vs. rest benchmark using 80MTI as OE for different choices of $h(z)$ in the radial function l of the HSC.

Data augmentation	$\ z\ _1$	$\ z\ _2$	$\ z\ _2^2$	$\sqrt{\ z\ ^2 + 1} - 1$
w/o	90.6	92.3	89.1	91.8
w/	92.5	94.1	94.5	96.1

set the weighting factor α to be $\alpha = 0.5$ [38]. Again note that $\gamma = 0$ corresponds to standard binary cross entropy. Figure 8 shows that mean AUC performance is insensitive to the choice of γ on the CIFAR-10 and ImageNet-1K one vs. rest benchmarks.

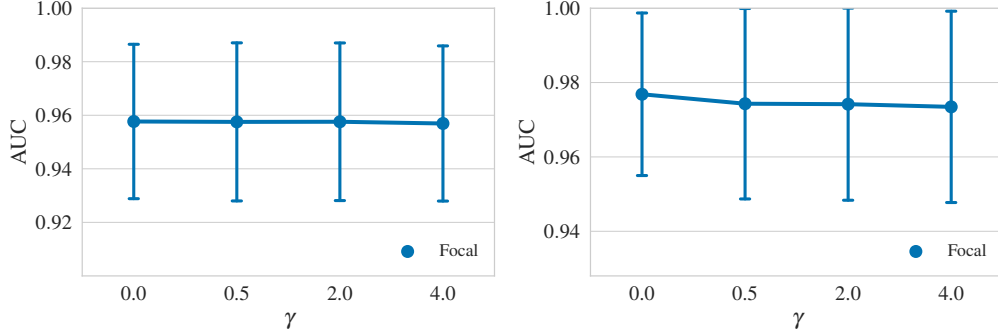


Figure 8: Focal loss detection performance in mean AUC in % when varying γ on the CIFAR-10 with 80MTI OE (left) and ImageNet-1K with ImageNet-22K OE (right) one vs. rest benchmarks.

D Network Architectures and Optimization

D.1 MNIST and CIFAR-10

On MNIST and CIFAR-10, we use LeNet-style networks having three convolutional layers and two fully connected layers. Each convolutional layer is followed by batch normalization, a leaky ReLU activation, and max-pooling. The first fully connected layer is followed by batch normalization, and a leaky ReLU activation, while the last layer is just a linear transformation. The number of kernels in the convolutional layers are, from first to last: 16-32-64 (MNIST), and 32-64-128 (CIFAR-10). The fully connected layers have 64-32 (MNIST), and 512-256 (CIFAR-10) units respectively. We use Adam [34] for optimization and balance every batch to contain 128 nominal and 128 OE samples during training. We train for 150 (MNIST) and 200 (CIFAR-10) epochs starting with a learning rate of $\eta = 0.001$ and have learning rate milestones at 50, 100 (MNIST), and 100, 150 (CIFAR-10) epochs. The learning rate is reduced by a factor of 10 at every milestone.

D.2 ImageNet

On ImageNet, we use exactly the same WideResNet [75] as was used in Hendrycks et al. [26], which has a ResNet-18 as architectural backbone. We use Adam [34] for optimization and balance every batch to contain 128 nominal and 128 OE samples during training. We train for 150 epochs starting with a learning rate of $\eta = 0.001$ and milestones at epochs 100 and 125. The learning rate is reduced by a factor of 10 at every milestone.

E Experimental Results on Individual Classes

For the CIFAR-10 one vs.-rest benchmark experiments from 4.1, we additionally report the standard deviations in Table 4. For the ImageNet-1K one vs.-rest benchmark experiments from 4.2, we present the performance over all classes with standard deviations in Table 5. For the experiments on varying

the number of OE samples, we include plots for all separate classes in Figure 9 for CIFAR-10 and in Figures 10–10 for ImageNet-1K respectively. Lastly for the experiments on varying the diversity of OE data on MNIST, with EMNIST-Letters OE, and CIFAR-10, with CIFAR-100 OE, we added plots for all separate classes as well in Figures 12 and 13.

Table 4: Detection performance in mean AUC in % (over 10 seeds) on the CIFAR-10 one vs. rest benchmark with 80MTI OE from Section 4.1 with standard deviations.

Class	— Unsupervised OE —		— Supervised OE —	
	Deep SAD	HSC	Focal	BCE
Airplane	94.2 ± 0.34	96.3 ± 0.13	95.9 ± 0.11	96.4 ± 0.17
Automobile	98.1 ± 0.19	98.7 ± 0.07	98.7 ± 0.09	98.8 ± 0.06
Bird	89.8 ± 0.54	92.7 ± 0.27	92.3 ± 0.32	93.0 ± 0.14
Cat	87.4 ± 0.38	89.8 ± 0.27	88.8 ± 0.33	90.0 ± 0.27
Deer	95.0 ± 0.22	96.6 ± 0.17	96.6 ± 0.10	97.1 ± 0.10
Dog	93.0 ± 0.30	94.2 ± 0.13	94.1 ± 0.21	94.2 ± 0.12
Frog	96.9 ± 0.22	97.9 ± 0.08	97.8 ± 0.07	98.0 ± 0.09
Horse	96.8 ± 0.15	97.6 ± 0.10	97.6 ± 0.16	97.6 ± 0.09
Ship	97.1 ± 0.21	98.2 ± 0.09	98.0 ± 0.11	98.1 ± 0.08
Truck	96.2 ± 0.22	97.4 ± 0.13	97.5 ± 0.12	97.7 ± 0.16
Mean AUC	94.4 ± 3.30	95.9 ± 2.68	95.7 ± 2.97	96.1 ± 2.71

Table 5: Detection performance in mean AUC in % (over 10 seeds) for all classes of the ImageNet-1K one vs. rest benchmark with ImageNet-22K OE from Section 4.2. This table corresponds to the results in Table 2, but here we report the performance on all individual classes and with standard deviations.

Class	— Unsupervised OE —		— Supervised OE —	
	Deep SAD	HSC	Focal	BCE
acorn	98.5 \pm 0.28	98.8 \pm 0.42	99.0 \pm 0.15	99.0 \pm 0.19
airliner	99.6 \pm 0.16	99.8 \pm 0.10	99.9 \pm 0.02	99.8 \pm 0.04
ambulance	99.0 \pm 0.13	99.8 \pm 0.13	99.2 \pm 0.14	99.9 \pm 0.07
american alligator	92.9 \pm 1.06	98.0 \pm 0.32	94.7 \pm 0.67	98.2 \pm 0.27
banjo	97.0 \pm 0.51	98.2 \pm 0.41	97.0 \pm 0.33	98.7 \pm 0.22
barn	98.5 \pm 0.29	99.8 \pm 0.05	98.7 \pm 0.24	99.8 \pm 0.08
bikini	96.5 \pm 0.84	98.6 \pm 0.57	97.2 \pm 0.89	99.1 \pm 0.30
digital clock	99.4 \pm 0.33	96.8 \pm 0.79	99.8 \pm 0.03	97.2 \pm 0.29
dragonfly	98.8 \pm 0.28	98.4 \pm 0.16	99.1 \pm 0.21	98.3 \pm 0.04
dumbbell	93.0 \pm 0.53	91.6 \pm 0.88	94.0 \pm 0.04	92.6 \pm 0.97
forklift	90.6 \pm 1.43	99.1 \pm 0.33	94.2 \pm 0.90	99.5 \pm 0.09
goblet	92.4 \pm 1.05	93.8 \pm 0.38	93.8 \pm 0.27	94.7 \pm 1.43
grand piano	99.7 \pm 0.06	97.4 \pm 0.37	99.9 \pm 0.04	97.6 \pm 0.34
hotdog	95.9 \pm 2.01	98.5 \pm 0.34	97.2 \pm 0.05	98.8 \pm 0.34
hourglass	96.3 \pm 0.37	96.9 \pm 0.26	97.5 \pm 0.17	97.6 \pm 0.48
manhole cover	98.5 \pm 0.29	99.6 \pm 0.34	99.2 \pm 0.09	99.8 \pm 0.01
mosque	98.6 \pm 0.29	99.1 \pm 0.26	98.9 \pm 0.30	99.3 \pm 0.15
nail	92.8 \pm 0.80	94.0 \pm 0.76	93.5 \pm 0.32	94.5 \pm 1.37
parking meter	98.5 \pm 0.29	93.3 \pm 1.64	99.3 \pm 0.04	94.7 \pm 0.76
pillow	99.3 \pm 0.14	94.0 \pm 0.47	99.2 \pm 0.14	94.2 \pm 0.42
revolver	98.2 \pm 0.30	97.6 \pm 0.25	98.6 \pm 0.11	97.7 \pm 0.68
rotary dial telephone	90.4 \pm 1.99	97.7 \pm 0.50	92.2 \pm 0.33	98.3 \pm 0.75
schooner	99.1 \pm 0.18	99.2 \pm 0.20	99.6 \pm 0.02	99.1 \pm 0.26
snowmobile	97.7 \pm 0.86	99.0 \pm 0.22	98.1 \pm 0.15	99.1 \pm 0.25
soccer ball	97.3 \pm 1.70	92.9 \pm 1.18	98.6 \pm 0.13	93.6 \pm 0.61
stingray	99.3 \pm 0.20	99.1 \pm 0.33	99.7 \pm 0.04	99.2 \pm 0.10
strawberry	97.7 \pm 0.64	99.1 \pm 0.20	99.1 \pm 0.03	99.2 \pm 0.22
tank	97.3 \pm 0.51	98.6 \pm 0.18	97.3 \pm 0.47	98.9 \pm 0.13
toaster	97.7 \pm 0.56	92.2 \pm 0.78	98.3 \pm 0.05	92.2 \pm 0.65
volcano	89.6 \pm 0.44	99.5 \pm 0.09	91.6 \pm 0.90	99.4 \pm 0.19
Mean AUC	96.7 \pm 2.98	97.3 \pm 2.53	97.5 \pm 2.43	97.7 \pm 2.34

Figure 9: Detection performance in mean AUC in % (over 10 seeds) for all classes of the CIFAR-10 one vs. rest benchmark from Section 4.1 when varying the number of 80MTI OE samples. These plots correspond to Figure 2, but here we report the results for all individual classes.

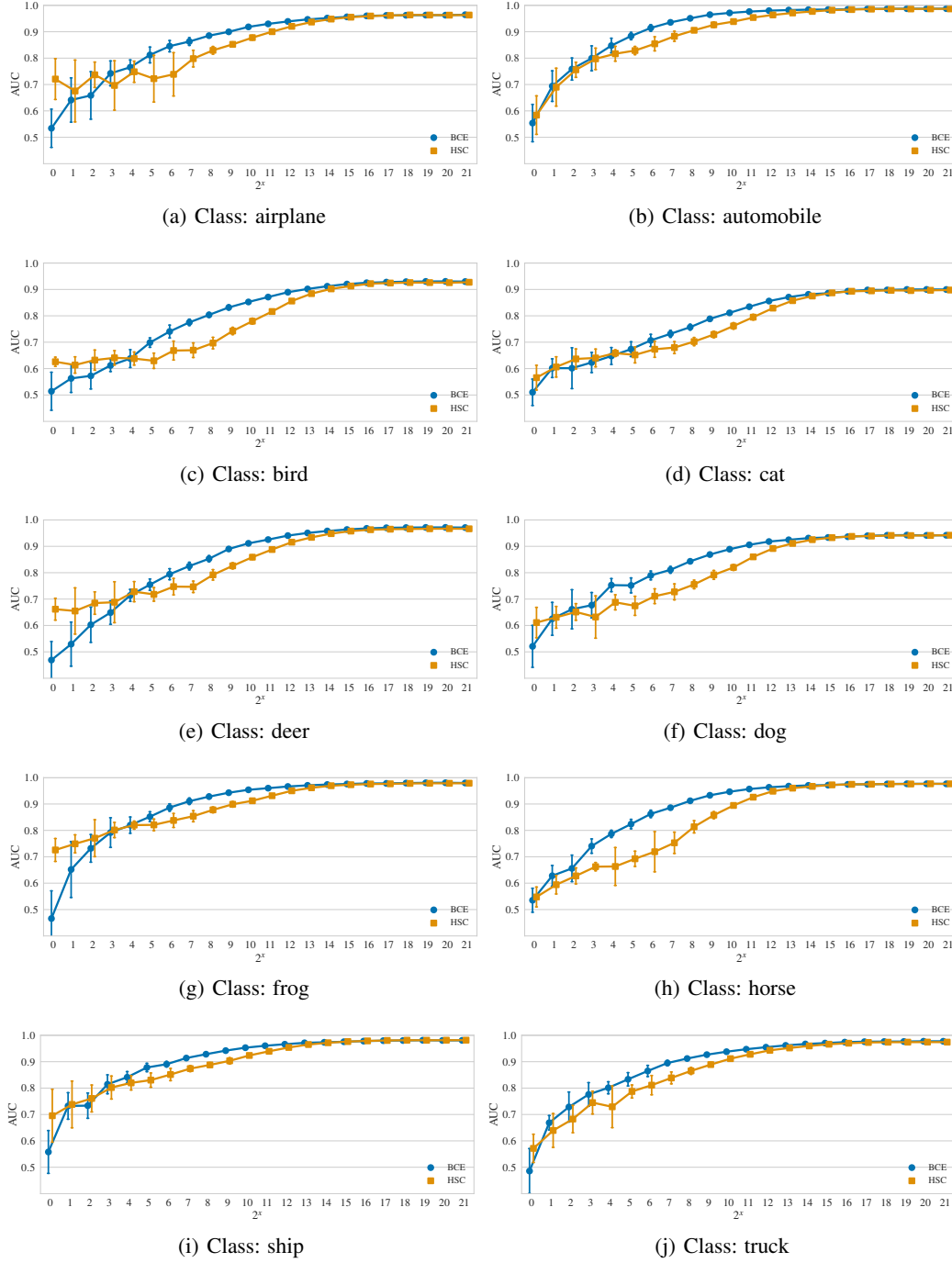


Figure 10: Detection performance in mean AUC in % (over 5 seeds) for all classes of the ImageNet-1K one vs. rest benchmark from Section 4.2 when varying the number of ImageNet-22K OE samples. These plots correspond to Figure 3, but here we report the results for all individual classes (from class 1 (acorn) to class 15 (hourglass)).

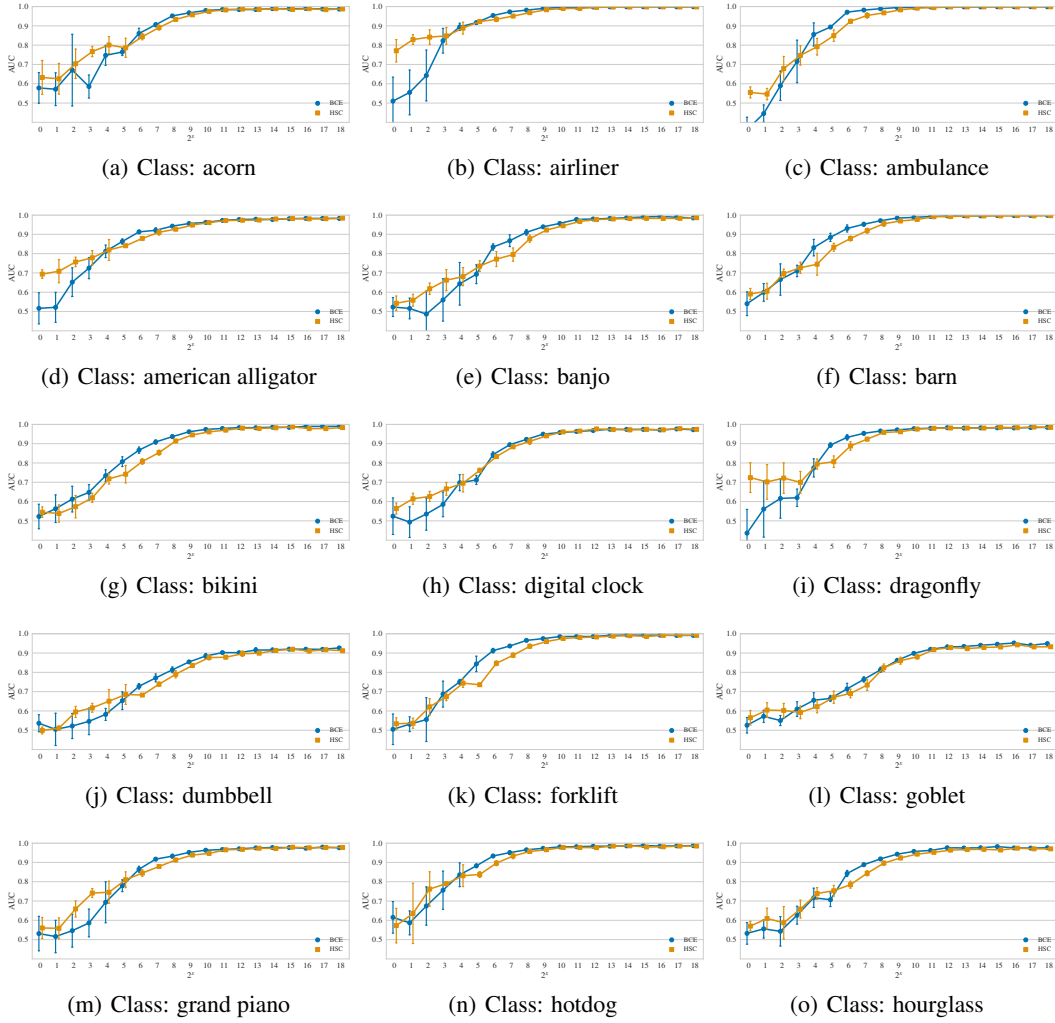


Figure 11: Detection performance in mean AUC in % (over 5 seeds) for all classes of the ImageNet-1K one vs. rest benchmark from Section 4.2 when varying the number of ImageNet-22K OE samples. These plots correspond to Figure 3, but here we report the results for all individual classes (from class 16 (manhole cover) to class 30 (volcano)).

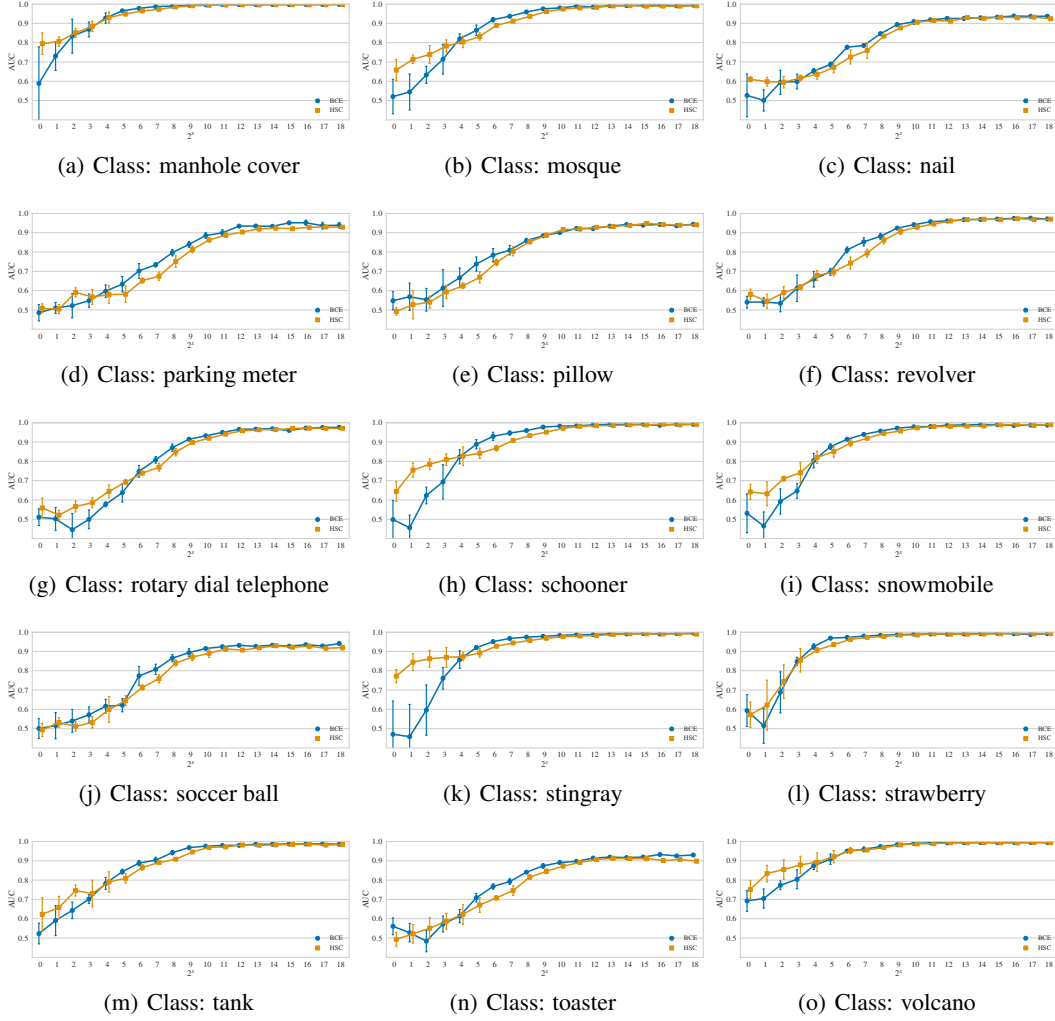


Figure 12: Detection performance in mean AUC in % (over 10 seeds) for all MNIST classes from the experiment in Section 4.3 on varying the number of classes k of the EMNIST-Letters OE data. These plots correspond to Figure 4 (left), but here we report the results for all individual classes.

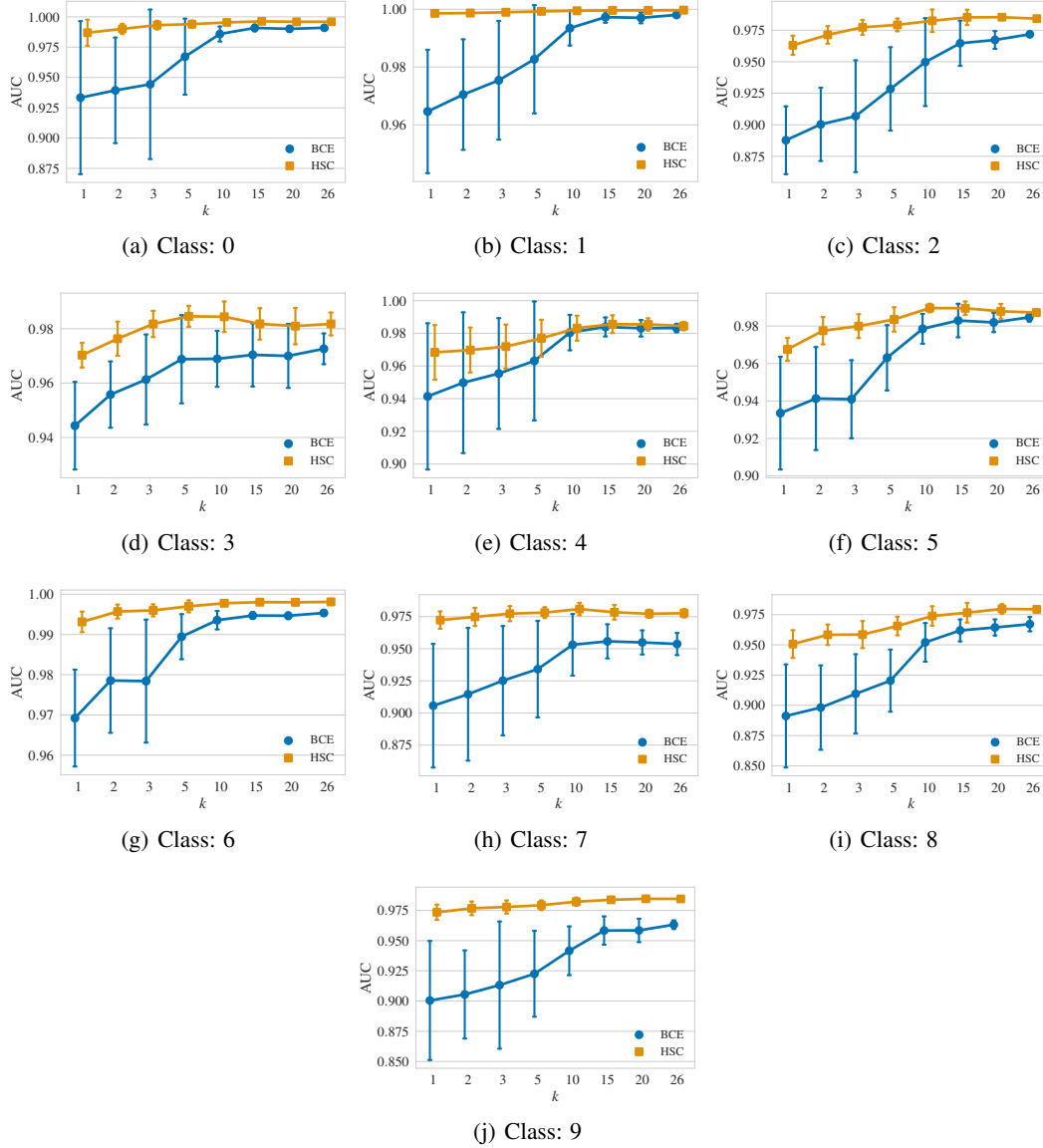


Figure 13: Detection performance in mean AUC in % (over 10 seeds) for all CIFAR-10 classes from the experiment in Section 4.3 on varying the number of classes k of the CIFAR-100 OE data. These plots correspond to Figure 4 (right), but here we report the results for all individual classes.

